Structural Durability & Health Monitoring
DOI:10.32604/sdhm.2020.08442
Article

Integrity Analysis on Existing Crane Runway Girders with Defects Using Constraint-Based R6 Criterion

Huajing Guo, Baijian Wu and Zhaoxia Li*

Jiangsu Key Laboratory of Engineering Mechanics, Department of Engineering Mechanics, Southeast University, Nanjing, 210096, China
*Corresponding Author: Zhaoxia Li. Email: zhxli@seu.edu.cn
Received: 25 August 2019; Accepted: 05 November 2019

Abstract: In order to resolve the safety problem of the existing crane runway girders (CRGs) with defects, the constraint-based R6 criterion is proposed to assess their structural integrity. The existing steel CRGs with defects at the weld joint between the upper flange and web plate, are characterized to three-dimensional finite element models with a semi-ellipse surface crack. The R6 criterion has been modified by considering the constraint effect which is represented by T-stress. The analysis results illustrate that working condition of the cracked CRGs leads to high constraint level along the crack front. The crack aspect ratio (a/c) and runway eccentricity (e) have significant influence on the integrity of the cracked CRGs. The integrity assessment results based on modified constraint-based R6 failure criterion enable to more effectively protect the cracked CRGs from brittle fracture failure.

Keywords: Crane runway girder; finite element; crack; structural integrity; constraint-based R6 failure criterion

1 Introduction

Fracture has been recognized as the elemental failure form of steel structures [1-4]. The research of the American Society of Civil Engineers showed that 80-90% of the failures in steel structures are related to fatigue and fracture [5]. The CRGs are the key components of steel structure plants which are subjected to cyclic loads caused by the periodical and frequent running of the cranes. Researches [6-8] indicated that failure of the CRGs usually occurs which could result in failure of the whole steel plant and the fatigue cracks often initiate at the weld joint between the upper flange and web plate of the CRGs. A steel CRG was detected to be failed due to a surface crack is showed as Fig. 1. In addition, another potential challenge to the CRGs is the runway eccentricity which could lead to crack initiation and propagation, even to brittle fracture [9].

Some efforts have been made on the stiffness and strength of CRGs of steel plants. Pi et al. [10] studied the nonuniform torsion of I-section beams by developing a large twist rotation inelastic model. Kennedy et al. [11] analyzed the capacity of the truss of steel crane girder system using non-linear incremental finite element method. Ren et al. [12] analyzed the elastic buckling coefficients of web plates of I-girders under patch load condition.

Figure 1: A failed steel CRG due to a surface crack at the weld joint between the upper flange and web plate

Up to now, the majority of researches focus on the fatigue lifetime of the steel CRGs. Liu et al. [13] put forward an analysis method to predict residual life of in-service steel crane structures by considering the influence of corrosion condition on fatigue resistance deterioration. Caglayan et al. [14] predicted the residual fatigue life of existing CRGs of a steel mill using quasi-static load tests and numerical analyses. Euler et al. [15] put forward local concepts to evaluate the fatigue problem of crane rail welds. Rettenmeier et al. [16] performed evaluation for fatigue lifetime of CRGs with consideration to the contribution of multiaxial stress state and the welding residual stresses.

However, fatigue cracks are usually detected in the in-service steel CRGs of the plants, while the researches are unable to assess the safety condition for the cracked CRGs. For example, the Miner law could be only used to analyze the fatigue issue of engineering structures without macro cracks [17]. As a result, although many researches have been performed, the fracture failure problem of the existing cracked CRGs has not been resolved yet. Therefore, integrity assessments for the existing cracked steel CRGs of plants using fitness-for-service method are urgently needed. Furthermore, the influence of the crack aspect ratio (a/c) and runway eccentricity (e) on the structural integrity should be studied.

According to the classical liner elastic fracture mechanics, only the singular stress near the crack tip contributes to the crack tip stress intensity factor K and stress paralleling to the crack plane has no effect on the K [18, 19]. However, the material fracture toughness may vary with the crack configurations (size and shape) and applied loading condition, including the stress triaxiality along crack front, which has been defined as constraint effect. Researches demonstrated that constraint effect has significant influence on the structural integrity [20, 21]. The stress triaxiality along crack front could be strengthened and the material fracture toughness be weakened under high constraint level condition. In contrast, the stress triaxiality could be reduced and the material fracture toughness be improved under the condition with low constraint level [22, 23].

Therefore, in order to solve the safety problems of existing CRGs with a semi-ellipse surface crack, constraint-based R6 failure criterion is proposed to assess the structural integrity of the cracked CRGs. The constraint effect level along crack front of CRGs has been quantified using T-stress and integrity analyses on cracked CRGs have been performed in which four groups of runway eccentricity (e = 0 mm, 11 mm, 21 mm and 41 mm) and three groups of crack aspect ratios (a/c = 1/2, 1.5/2 and 2/2) have been studied in the paper.

2 Fracture Theories and Methods

2.1 Theories of Stress Intensity Factor and T-Stress

Irwin [24] put forward the stress intensity factor K to present the crack tip fields which is the function of applied loading and crack configurations (size, shape and orientation). In a polar coordinate system (r, θ) with

the origin being at crack tip, the full Williams expansion of the stress field in the vicinity of a crack can be expressed as [25]:

$$\sigma_{ij} = Ar^{-1/2} f_{ij}(\theta) + Bg_{ij}(\theta) + Cr^{1/2} h_{ij}(\theta) + \ldots \tag{1}$$

where σ_{ij} is stress, r is the distance from the crack tip, the functions $f_{ij}(\theta)$, $g_{ij}(\theta)$, $h_{ij}(\theta)$ are functions of a point, and A, B and C are the parameters whose magnitude are proportional to the remotely applied load.

T-stress has been equally treated as the stress paralleling to the crack plane which is utilized to quantify constraint effect in the vicinity of a crack tip. Researches [20, 21] illustrated that positive T-stress value implies high constraint level and negative T-stress value stands for low constraint level. *K-T* theory only considers the first (singular) and second (non-singular) term:

$$\sigma_{ij} = \frac{K_{\mathrm{I}}}{\sqrt{2\pi r}} f_{ij}(\theta) + T\delta_{1i}\delta_{1j} \tag{2}$$

where δ_{ij} is Kronecker delta, K_{I} is mode I linear stress intensity factor, T is T-stress.

Toshio et al. [26] put forward the interaction integral method to extract the elastic T-stress which is related to a domain integral I (s):

$$I(s) = \frac{1}{A_c} \int\limits_{V(s)} \left[\left(\sigma_{ij} \frac{\partial u_i{}^L}{\partial x_k} + \sigma_{ij}^L \frac{\partial u_i}{\partial x_k} \right) \frac{\partial q_k}{\partial x_j} - \sigma_{ij}^L \varepsilon_{ij} \frac{\partial q_k}{\partial x_k} \right] dV \tag{3}$$

where $u_i{}^{\mathrm{L}}$ is auxiliary displacement, $\sigma_{ij}{}^{\mathrm{L}}$ is auxiliary stress, q defines the virtual extension of the crack front segment and A_{c} is the increase in crack area generated by the virtual crack advance.

Therefore, the expression of T-stress can be obtained as [26]:

$$T(s) = -\frac{E}{1-v^2} \left[\frac{I(s)}{f} + v\varepsilon_{33}(s) \right] \tag{4}$$

where f is the applied point force, v is Poisson's ratio $\varepsilon_{33}(s)$ is the tangential strain at point s in the crack front.

The finite element method enables to calculate the value of K and T-stress based on stress or displacement distributions around the crack front [27]. In the paper, the values of K and T-stress are extracted from commercial code ABAQUS directly.

2.2 Constraint-Based R6 Criterion

The R6 failure criterion was proposed by Central Electricity Generating Board (CEGB) of UK and it has been widely applied to structural integrity assessment using failure assessment diagram (FAD) [28]. The horizontal and vertical axes of FAD are labeled by L_r and K_r, respectively. Milne et al. [29] defined two parameters K_r and L_r as:

$$K_r = K(P, a)/K_{mat} \tag{5}$$

$$L_r = P/P_L(a, \sigma_y) \tag{6}$$

where $K(P, a)$ is the linear elastic stress intensity factor, K_{mat} is the material fracture resistance, a is crack size, P represents the magnitude of the applied load, and $P_L(a, \sigma_y)$ is the corresponding magnitude at plastic collapse for yield stress.

The failure assessment curve (FAC) of R6 has three options and the K_r can be expressed as the function of L_r, namely $f(L_r)$. The FAC can be obtained using one of the three options of R6, which enables to

differentiate safe working condition from failure condition. In the FAD, the safe area means that all the points (K_r, L_r) in the area lie in the inner of the failure curves [28].

Option 1:

$$K_r = f_1(L_r) = \left(1 - 0.14{L_r}^2\right)\left(0.3 + 0.7\exp\left(-0.65{L_r}^6\right)\right) \tag{7}$$

Option 2:

$$K_r = f_2(L_r) = \left(\frac{E\varepsilon_{ref}}{L_r\sigma_y} + \frac{{L_r}^3\sigma_y}{2E\varepsilon_{ref}}\right)^{-0.5} \tag{8}$$

Option 3:

$$K_r = f_3(L_r) = \sqrt{\frac{J_e}{J}} \tag{9}$$

where E is Young's modulus, ε_{ref} is the uniaxial strain at a reference stress and σ_y is the yield stress, J is J-integral, J_e is elastic J-integral.

The option 1 curve is independent of both material and geometry of structures, which approaches to the option 2 curve when realistic stress/strain data of parent steel and weld metal is used [30]. Considering the constraint effect along crack front, the failure assessment curves can be modified as:

$$K_r = f(L_r)\left(\frac{K^c_{mat}}{K_{mat}}\right) \tag{10}$$

where the K^c_{mat} denotes the material constraint-dependent fracture toughness value and can be expressed as [31]:

$$K^c_{mat} = K_{mat}[1 + \alpha_0(\beta L_r)] \tag{11}$$

$$\beta = \frac{T}{\sigma_y L_r} \tag{12}$$

where the function α_0 describes the elevation of toughness.

The positive T-stress implies that the material fracture toughness could be weakened and negative T-stress implies reinforced fracture toughness. The more positive the T-stress causes to the greater increase of compressive stress triaxiality [20, 21]. Therefore, the following equation can be obtained:

$$\begin{cases} \dfrac{K^c_{mat}}{K_{mat}} < 1, & \text{T}-\text{stress is positive} \\ \dfrac{K^c_{mat}}{K_{mat}} > 1, & \text{T}-\text{stress is negative} \end{cases} \tag{13}$$

Combining Eqs. (11) and (12) with Eq. (10), the modified option 1 of R6 can be obtained as

$$K_r = f_1(L_r) = \left(1 - 0.14{L_r}^2\right)\left(0.3 + 0.7\exp\left(-0.65{L_r}^6\right)\right)\left(1 + \alpha_0\left(\frac{T}{\sigma_y}\right)\right) \tag{14}$$

In the paper, the R6 failure criterion is modified by considering the constraint effect which is represented by T-stress. The integrity analysis on the existing CRGs with defects have been performed using the constraint-based R6 criterion. The technique flow chat of the paper is illustrated as Fig. 2.

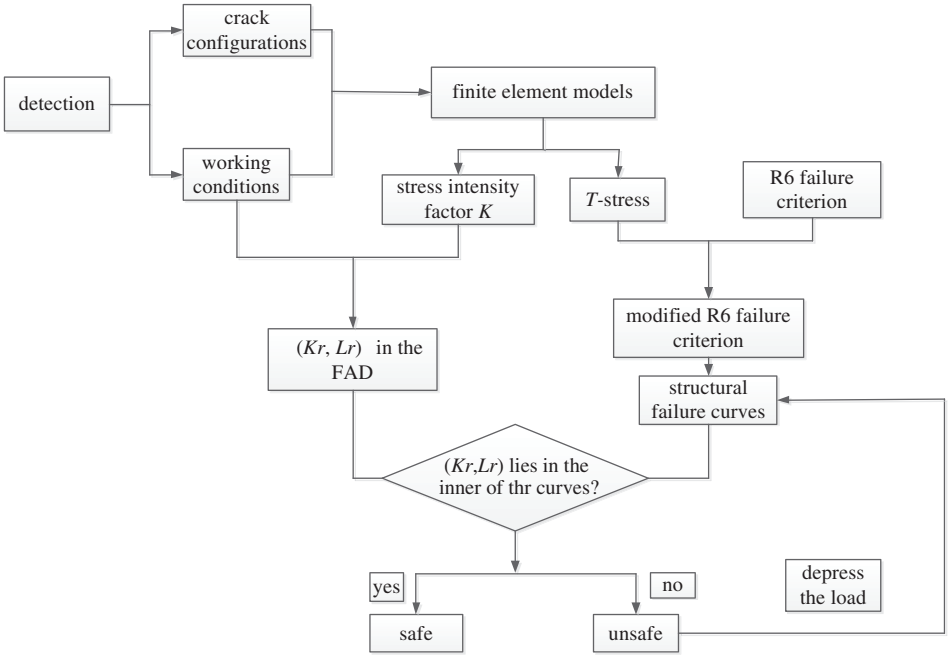

Figure 2: Technique flow chat of the work

3 Models of In-Service CRGs of Steel Plants

3.1 Configurations of Steel CRGs

The CRGs support the crane running on it in the lifetime and a view of the working background of CRGs of a steel plant is showed as Fig. 3(a). The CRG system can be simply illustrated as Fig. 3(b) and the configurations of the CRG are showed as Fig. 3(c, d). In the paper, the basic properties of the CRGs are obtained from the round billet caster of a steel plant which has served for nearly twenty years [32]. The crane is a soft hook bridge one with sixteen wheels (190t/50t, A7) and the mechanical property and distribution of wheels of the crane are showed as Tab. 1 and Fig. 4, respectively. Steel Q345 usually has been made to CRGs for its high strength and the material mechanical properties are listed as Tab. 2.

3.2 Finite Element Models of CRGs with a Semi-Ellipse Surface Crack

In practice, the rail misalignment, crane move and other out-of plane distortions often lead to runway eccentricity which jeopardizes the integrity of CRGs, even causes brittle fracture [33, 9]. Special attention should be paid to the horizontal force caused by the swing of cranes. According to China's code for design of steel structures, the value of horizontal force acting at each wheel can be expressed as [34]:

$$P_x = \alpha P_{kmax} \tag{15}$$

where the P_{kmax} is the maximal static wheel load, α is crane property parameter and $\alpha = 0.1$ in the paper. Note that all of the Max static wheel load $P_{kmax}(i) = 450$ kN ($i = 1, 2, 3, 4, 5, 6, 7, 8$) and the horizontal rail force $P_x = 45$ kN in the later analysis.

In the study, the CRGs are simplified as three-dimensional models which contains only the key features of the actual CRGs with appropriate assumptions. Therefore, it is assumed that the weld joint between the upper flange and web plate exists a semi-ellipse surface crack. The three-dimensional numerical simulation analyses are performed using ABAQUS, and element type 8-node linear brick incompatible

(a) a steel plant

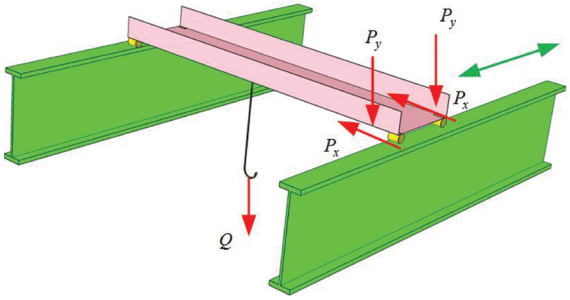

(b) the simplified CRG system

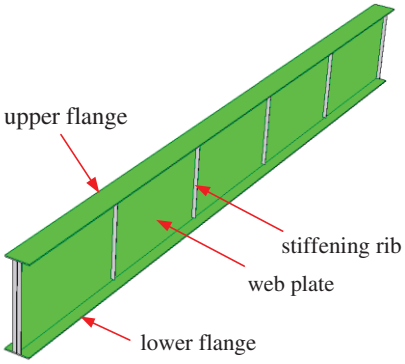

(c) the construction of a CRG

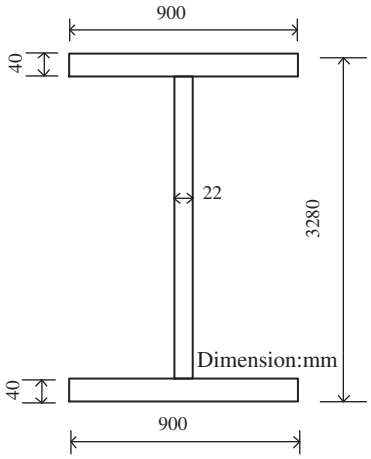

(d) the cross section of the CRG

Figure 3: Physical model of the CRG

Table 1: The wheel loads of the cranes

Wheel	p1	p2	p3	p4	p5	p6	p7	p8
Max static wheel load /kN	450	450	450	450	450	450	450	450
Min static wheel load /kN	195	205	205	195	190	200	200	190

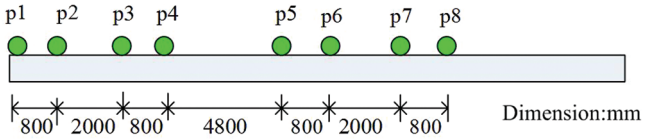

Figure 4: Distributions of crane wheels

modes (C3D8I) is selected for stress analysis. The tie interaction has used to simulate the weld connection between components, such as the connection between flanges and web plate, stiffening rib and web plate. By taking advantage of structural symmetry, only half of the CRGs system are simulated. Symmetric conditions are applied to the two sides of the CRG model and the partial underside of CRG is fixed.

Table 2: Mechanical properties of steel Q345

Material	Yield stress (σ_y)	Elastic modulus (E)	Poisson's ratio (μ)
Q345	345 MPa	206 GPa	0.3

Three groups of crack aspect ratios (a/c = 1/2, 1.5/2 and 2/2) under different runway eccentricity have been analyzed. To be concise, only the finite element model of the cracked CRG with a = 1 mm, c = 2 mm is showed as Fig. 5, including 58682 nodes and 52831 elements. K and T-stress are computed based on the domain integral by using six contours around the crack tip in this study.

The maximum midspan displacement is usually used to represent the working condition of CRGs. In the numerical analyses, let the vertical static wheel load $P_{(i)}$ = 450 kN (i = 1, 2, 3, 4, 5, 6, 7, 8) and the maximum midspan displacement has been obtained as 14.5 mm, shown as Fig. 6. Under the same condition, the measured midspan displacement is 15 mm, including the arch camber [32, 34]. The relative difference value is 3.33%, which illustrated the developed finite element models for CRGs are reliable.

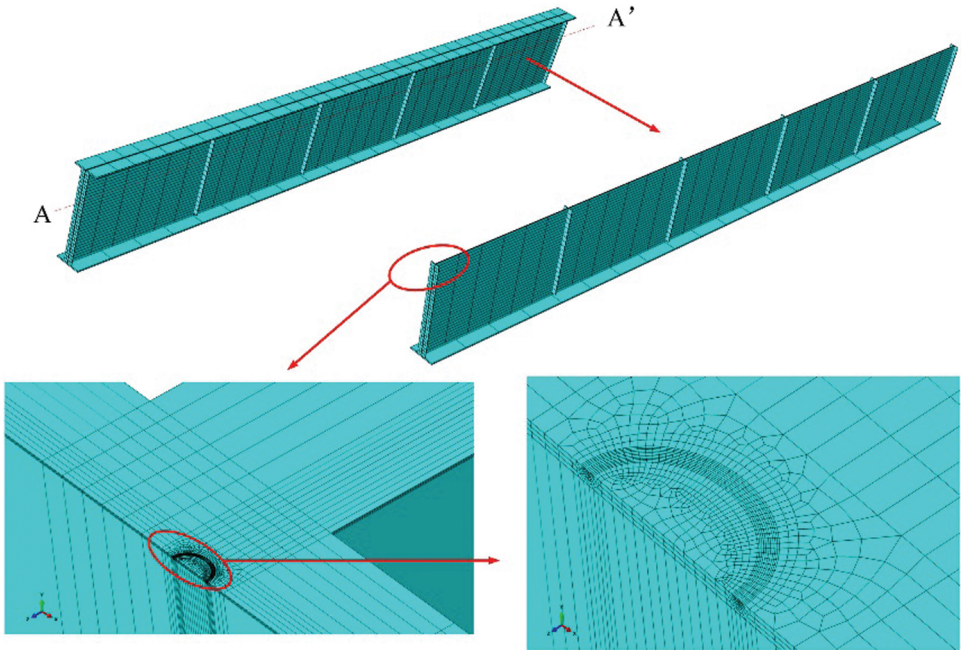

Figure 5: Finite element model of a cracked CRG

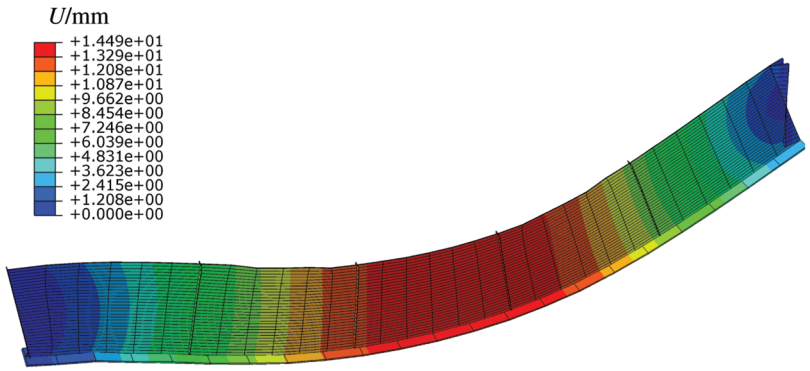

Figure 6: Displacement of the cracked CR

4 Numerical Analysis Results of Cracked CRGs

4.1 Distributions of K

The influence of aspect ratio (a/c) and runway eccentricity (e) on the distributions of K along the crack front have been studied, respectively. The numerical analysis results are showed as Figs. 7 and 8, the following conclusions can be drawn: The position $\theta = 0°$ may be the most dangerous position with the maximum K value; The value of K increases with the increase of the runway eccentricity (e) and/or aspect ratio (a/c), except a few area with low stress level.

4.2 Analysis Results of Constraint Effect

The constraint effect in the vicinity of crack of the CRGs is represented by T-stress and the influence of crack aspect ratio and runway eccentricity on the T-stress have been studied, respectively. The numerical analysis results are showed as Figs. 9 and 10, which enables to draw the following conclusions: The T-stress value of the crack front almost keeps positive, which illustrates high constraint level along the crack front; The maximum T-stress value always occurs at the position $\theta = 0°$, which implies the position $\theta = 0°$ is the dangerous position; The T-stress value at the dangerous position increases with the increase of the aspect ratio (a/c) and/or runway eccentricity (e).

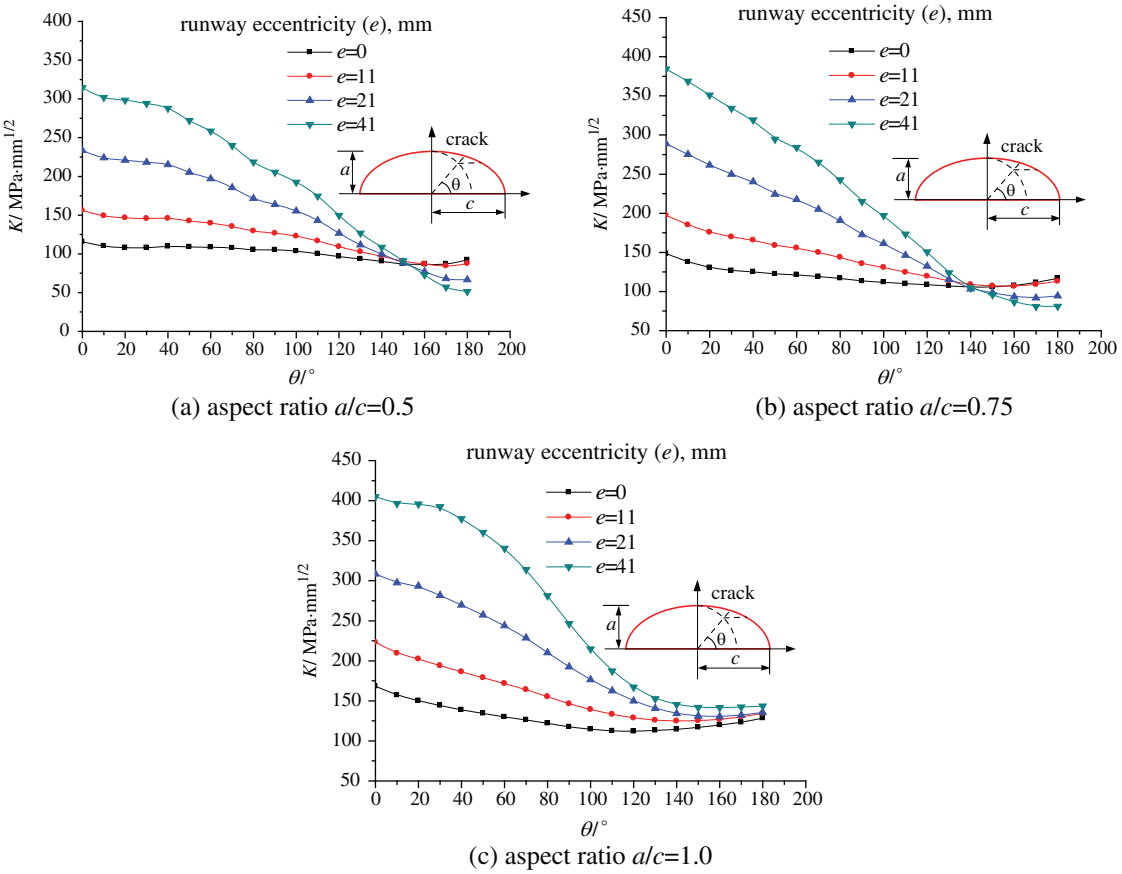

(a) aspect ratio a/c=0.5

(b) aspect ratio a/c=0.75

(c) aspect ratio a/c=1.0

Figure 7: Distributions of K of cracked CRGs with different aspect ratio

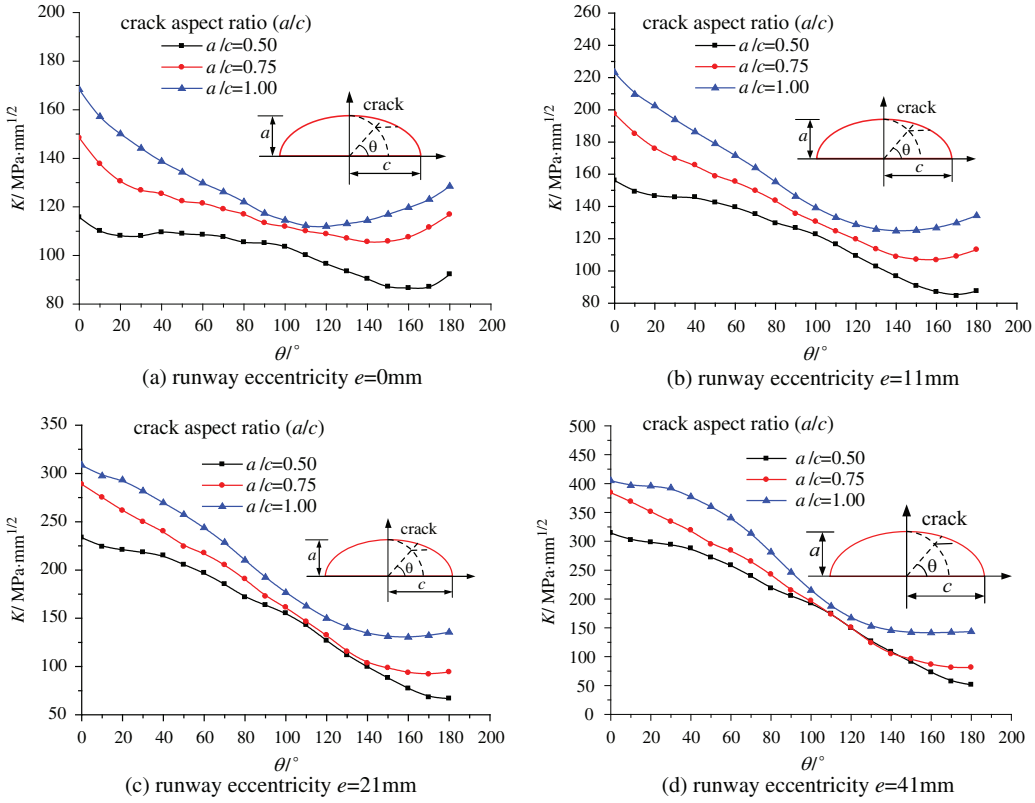

Figure 8: The distributions of K of cracked CRGs subjected to eccentric loading

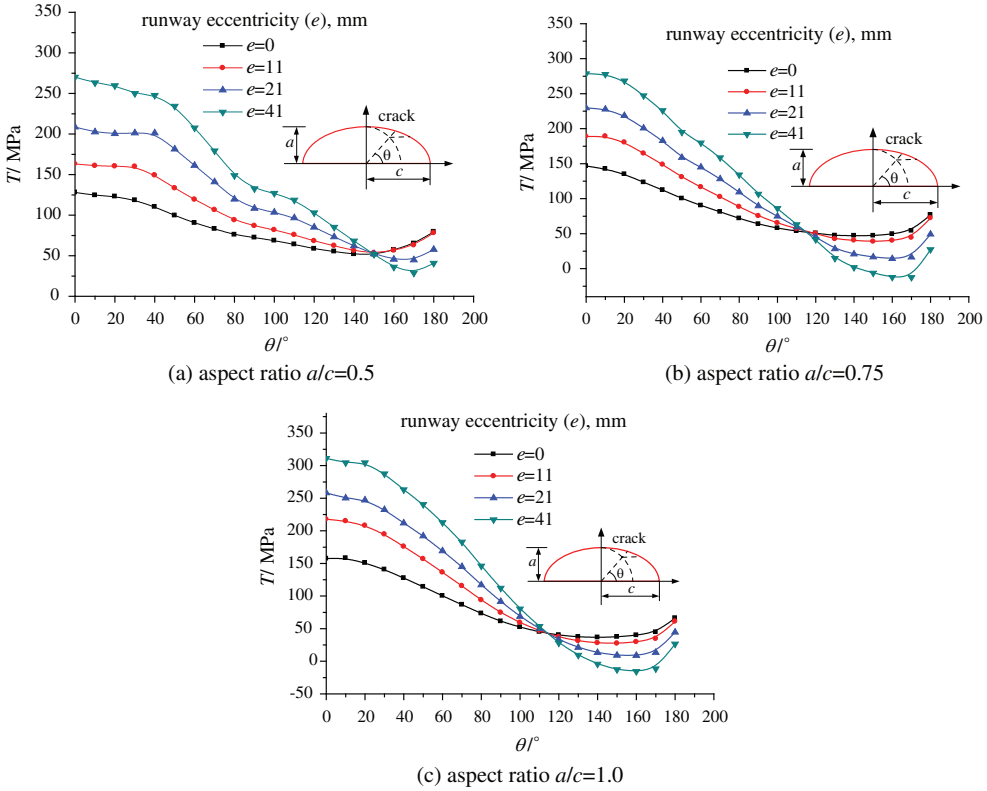

Figure 9: Distributions of T-stress of cracked CRGs with different aspect ratio

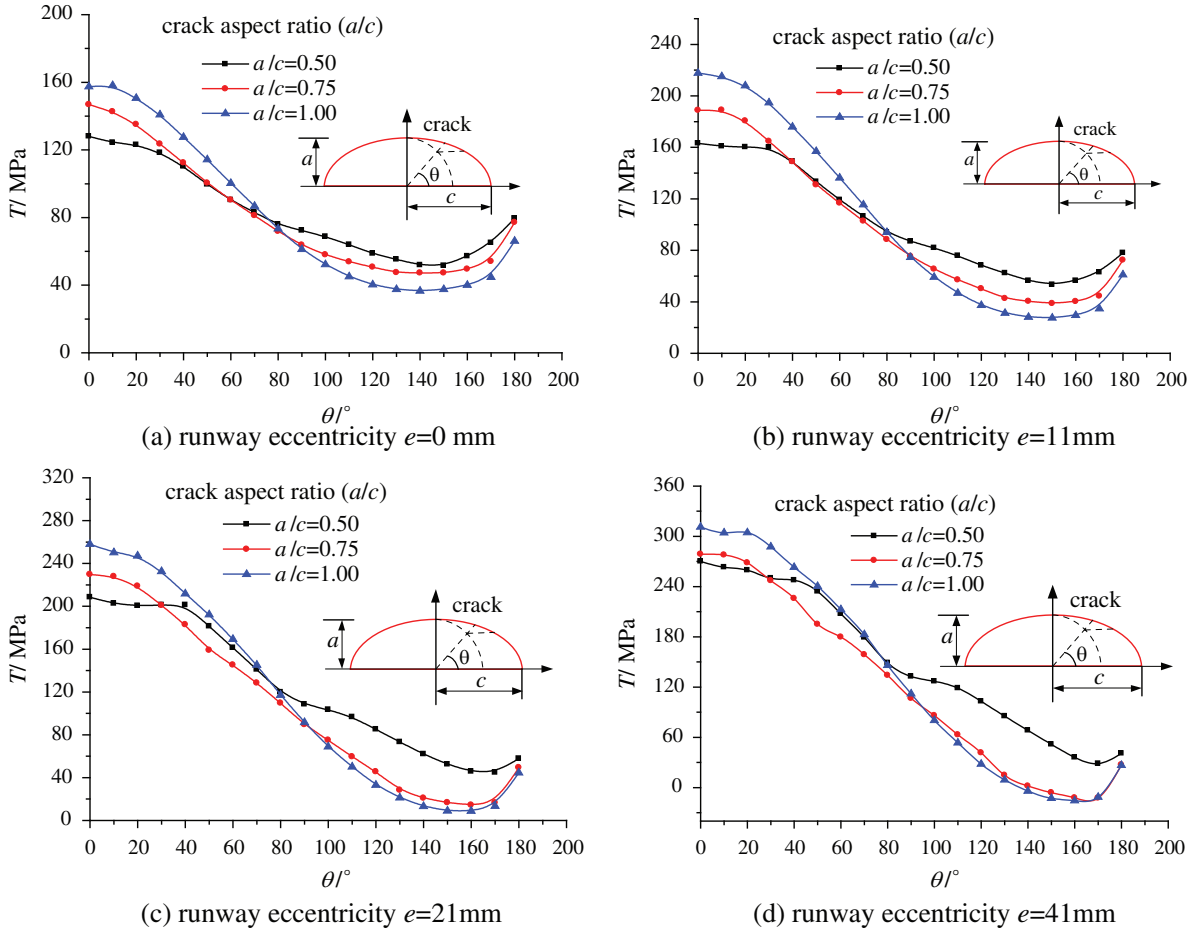

(a) runway eccentricity e=0 mm (b) runway eccentricity e=11mm

(c) runway eccentricity e=21mm (d) runway eccentricity e=41mm

Figure 10: Distributions of T-stress of cracked CRGs subjected to different eccentric loading

5 Integrity Assessment for Cracked CRGs

It can be obtained from the Section 4.1 and Section 4.2 that the position point $\theta = 0°$ along the crack front is the dangerous position with maximal value of stress level (K) and constraint level (T-stress). As a result, fracture failure of cracked CRGs may occur at the area near by the point θ = 0°. Therefore, the integrity assessments on the dangerous position of a series of cracked CRGs have been performed using both R6 criterion and constraint-based R6 criterion in which the influence of the runway eccentricity and crack aspect ratio on the FACs have been studied, respectively.

The option 1 of constraint-based R6 is used for the integrity assessments for the cracked CRGs. The expression in its the simplest form is illustrated as the following equation:

$$K_r = f_1(L_r) = \left(1 - 0.14{L_r}^2\right)\left(0.3 + 0.7\exp\left(-0.65{L_r}^6\right)\right)\left(1 - 0.5\beta L_r\right) \tag{16}$$

The maximal and minimum wheel load of the crane are designed and the applied load has to range from the minimum to maximal. Therefore, in terms of being simple and convenient for the application, make the p_0 = P_{max} = 450 kN and p ranges from 210 kN to 450 kN.

The following conclusions can be drawn based on numerical results showed in Fig. 11: the constraint-based R6 criterion takes the runway eccentricity and crack configuration into consideration and the safe area in the FAD decreases with the increase of the runway eccentricity; The assessment results based on modified constraint-based R6 failure criterion enable to more effectively protect the cracked CRGs from brittle fracture failure. Take the points in Fig. 11(a) whose the horizontal axis L_r = 0.71 (P_y = 320 kN) as an example, the relative difference value K_r is approximately 34% with the maximum value K_rmax = 0.88 and minimum K_rmin = 0.58.

According to the results showed in the Fig. 12, the following conclusions can be drawn: the safe area decreases with the increase of the aspect ratio when the length of major semi-axis (c) of surface crack is fixed; The studied three groups of cracked CRGs are in good condition. For example, the most serious condition happens when the parameters arrive at the critical value, namely a/c = 1 and P_{y0} = P_{ymax}, showed as the point A (K_{rA}, L_{rA}) in Fig. 12(d). Note that K_{IC} = 1612 MPa·mm$^{1/2}$ and K_0 = 405 MPa·mm$^{1/2}$. Therefore, the value K_{rA} is 0.25 and the critical value is 0.31, which implies that the cracked CRGs are in good condition.

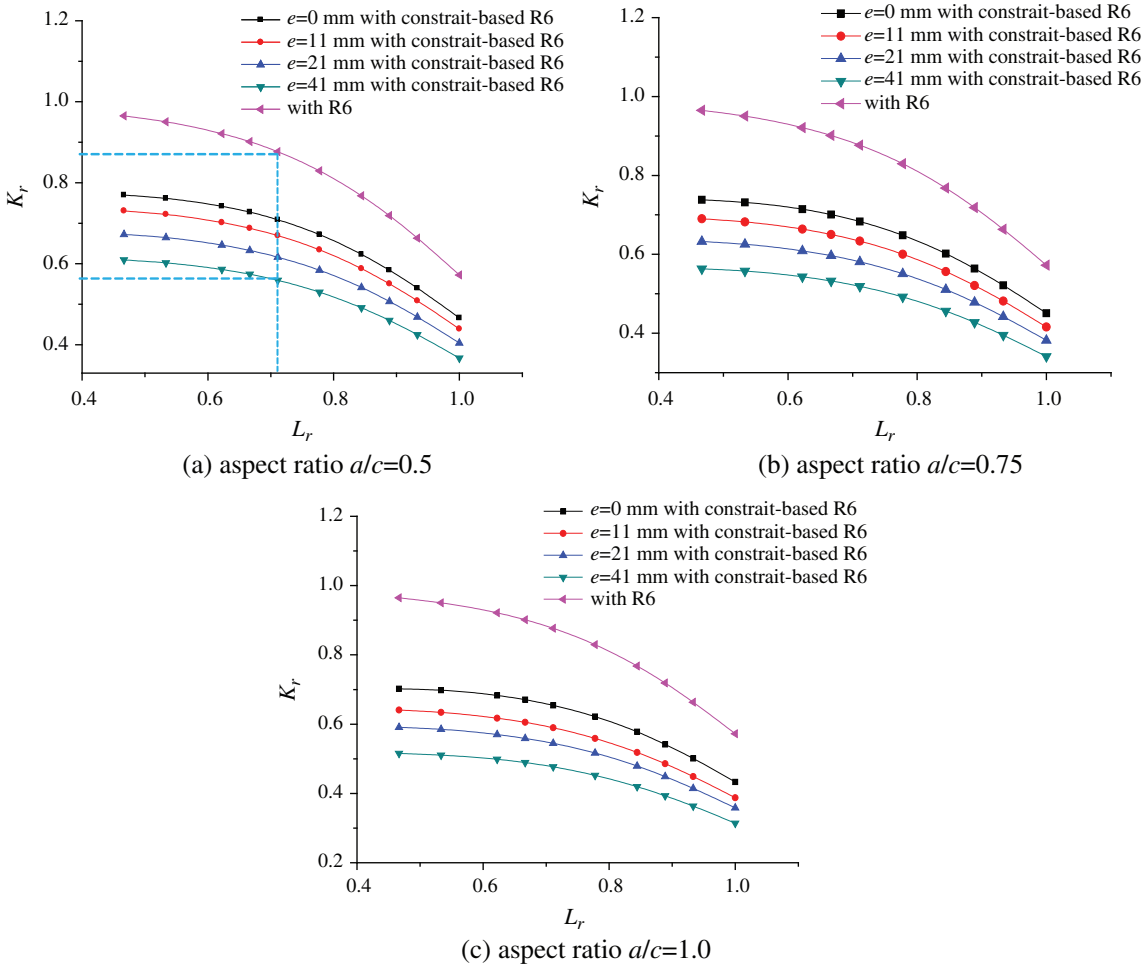

(a) aspect ratio a/c=0.5

(b) aspect ratio a/c=0.75

(c) aspect ratio a/c=1.0

Figure 11: Comparisons between FACs with R6 and constraint-based R6

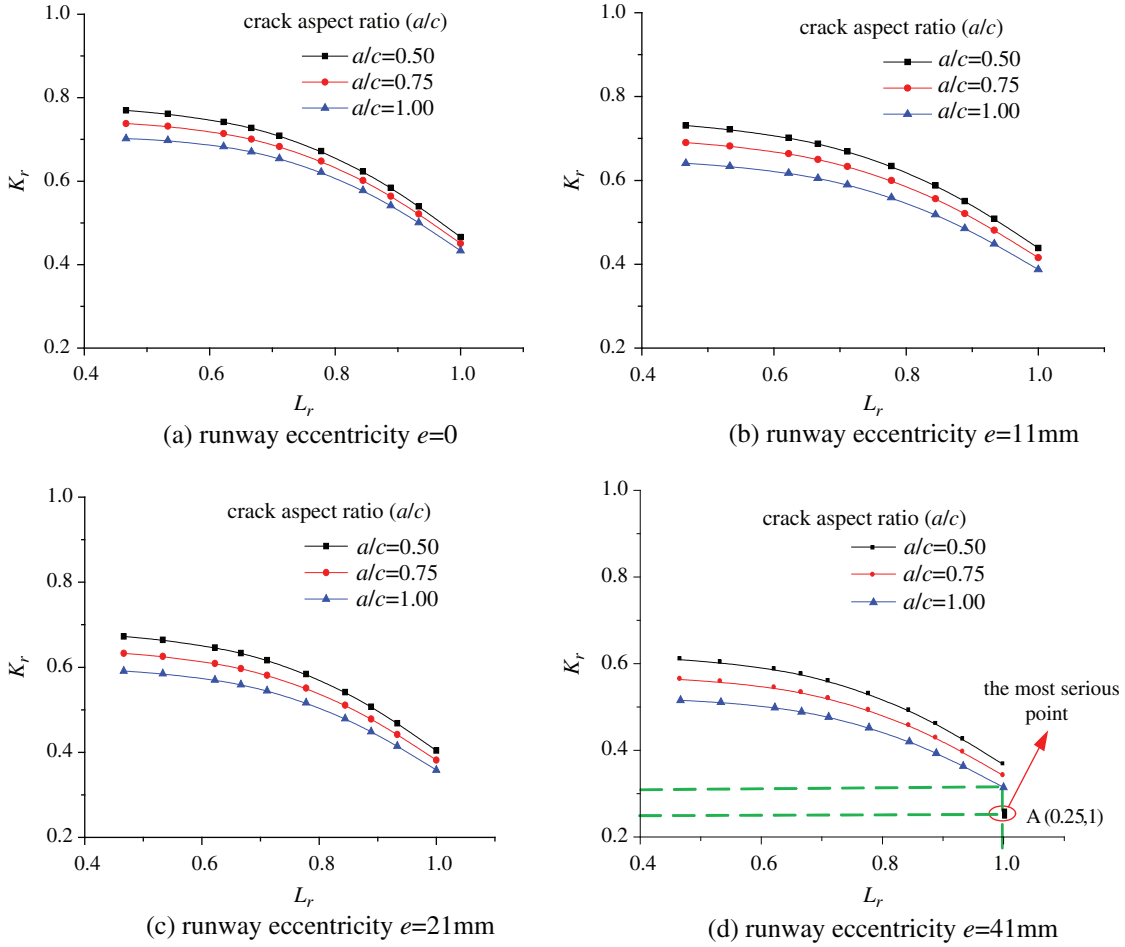

(a) runway eccentricity e=0 (b) runway eccentricity e=11mm

(c) runway eccentricity e=21mm (d) runway eccentricity e=41mm

Figure 12: FADs of CRGs subjected to eccentric loading with constraint-based R6 criterion

6 Conclusions

In order to resolve the safety problem of the existing the cracked steel CRGs, the constraint-based R6 criterion is proposed to assess their structural integrity. Integrity assessments have been performed for a series of cracked CRGs using both R6 criterion and constraint-based R6 criterion and comparisons have been made between the two kinds of results. The main conclusions are listed as following:

1. The working condition of the cracked CRGs leads to high constraint level along the crack front which could lead to stress triaxiality increased and fracture toughness reduced.
2. The constraint level of the cracked CRGs increases with increase of crack aspect ratio (a/c) and/or runway eccentricity (e).
3. The integrity assessment results based on modified constraint-based R6 failure criterion enable to more effectively protect the cracked CRGs from brittle fracture failure.
4. The studied CRGs with a surface crack are in good condition. The crack aspect ratio (a/c) and runway eccentricity (e) have significant influence on the structural integrity of the cracked CRGs.

Funding Statement: The works described in this paper are financially supported by the National Program on Key Research Project (2016YFC0701301-02), to which the authors are most grateful.

Conflicts of Interest: The authors declared no potential conflicts of interest with respect to the research, authorship, and/or publication of this article.

References

1. Duchaczek, A., Mańko, Z. (2017). Influence of the holes spacing in bolted connections on propagation of fatigue cracks in steel bridge girders. *KSCE Journal of Civil Engineering, 21(3),* 838–850. DOI 10.1007/s12205-016-0566-6.
2. Ko, Z. G., Lee, H., Bin, W., An, Z., Chung, W. (2017). An experimental study on joint performance of steel I-girders connected to inverted-T bent cap in fatigue testing. *KSCE Journal of Civil Engineering, 21(7),* 2828–2836. DOI 10.1007/s12205-017-1373-4.
3. Liu, J. P., Zhang, L. X., Zhang, H. H., Liu, T. (2019). Seismic vulnerability analysis of single-story reinforced concrete industrial buildings with seismic fortification. *Structural Durability and Health Monitoring, 13(2),* 123–142. DOI 10.32604/sdhm.2019.04486.
4. Zhao, Y., Noori, M., Altabey, W. A., Ghiasi, R., Wu, Z. S. (2019). A fatigue damage model for FRP composite laminate systems based on stiffness reduction. *Structural Durability and Health Monitoring, 13(1),* 85–103. DOI 10.32604/sdhm.2019.04695.
5. ASCE. (1982). Committee on fatigue and fracture reliability of the committee on structural safety and reliability of the structural division, fatigue reliability l-4. *Journal of Structural Engineering-ASCE, 108(1),* 3–88.
6. Rettenmeier, P., Roos, E., Weihe, S. (2016). Fatigue analysis of multiaxially loaded crane runway structures including welding residual stress effects. *International Journal of Fatigue, 82*, 179–187. DOI 10.1016/j.ijfatigue.2015.04.009.
7. Wardenier, J., de Vries, P., Timmermann, G. (2017). Evaluation of cracks in an offshore crane runway girder. *Steel Construction, 10(1),* 67–71. DOI 10.1002/stco.201710011.
8. Yue, Q. R., Xing, K. T., Zheng, Y. (2017). *Evaluation and strengthening of fatigue performance for steel crane girders system*. China: China Building Industry Press (In Chinese).
9. Graciano, C., Uribe-Henao, A. F. (2014). A strength of steel I-girders subjected to eccentric patch loading. *Engineering Structures, 79(1),* 401–406. DOI 10.1016/j.engstruct.2014.08.031.
10. Pi, Y. L., Trahair, N. S. (1995). Inelastic torsion of steel I-beams. *Journal of Structural Engineering, 121(4),* 609–620. DOI 10.1061/(ASCE)0733-9445(1995)121:4(609).
11. Kennedy, D. J. L., Albert, C., Maccrimmon, R. A. (2000). Inelastic incremental analysis of an industrial pratt truss. *Engineering Structures, 22(2),* 146–154. DOI 10.1016/S0141-0296(98)00104-7.
12. Ren, T., Tong, G. S. (2005). Elastic buckling of web plates in I-girders under patch and wheel loading. *Engineering Structures, 27(10),* 1528–1536. DOI 10.1016/j.engstruct.2005.05.006.
13. Liu, H. B., Xing, K. T. (2005). Assessment of fatigue reliability of steel crane structures in service based on damage cumulative model. *Proceedings of the Fourth International Conference on Advances in Steel Structures, II,* 1121–1126.
14. Caglayan, O., Ozakgul, K., Tezer, O., Uzgider, E. (2010). Fatigue life prediction of existing crane runway girders. *Journal of Constructional Steel Research, 66(10),* 1164–1173. DOI 10.1016/j.jcsr.2010.04.009.
15. Euler, M., Kuhlmann, U. (2011). Crane runways – fatigue evaluation of crane rail welds using local concepts. *International Journal of Fatigue, 33(8),* 1118–1126. DOI 10.1016/j.ijfatigue.2011.02.010.
16. Rettenmeier, P., Roos, E., Weihe, S., Schuler, X. (2016). Assessment of mixed mode crack propagation of crane runway girders subjected to cyclic loading. *Engineering Fracture Mechanics, 153,* 11–24. DOI 10.1016/j.engfracmech.2015.12.018.
17. Miner, M. A. (1945). Cumulative damage in fatigue. *Journal of Applied Mechanics-Transactions of the ASME, 67*, A159–A164.
18. Eftis, J., Subramonian, N., Liebowitz, H. (1977). Crack border stress and displacement equations revisited. *Engineering Fracture Mechanics, 9(1),* 189–210. DOI 10.1016/0013-7944(77)90063-7.

19. Eftis, J., Subramonian, N. (1978). The inclined crack under biaxial load. *Engineering Fracture Mechanics, 10(1),* 43–67. DOI 10.1016/0013-7944(78)90049-8.
20. Qian, G. A., Niffenegger, M. (2013). Integrity analysis of a reactor pressure vessel subjected to pressurized thermal shocks by considering constraint effect. *Engineering Fracture Mechanics, 112,* 14–25. DOI 10.1016/j.engfracmech.2013.09.009.
21. Liu, S., Wang, G. Z., Tu, S. T., Xuan, F. Z. (2016). Creep crack growth prediction and assessment incorporating constraint effect for pressurized pipes with axial surface cracks. *Engineering Fracture Mechanics, 154,* 92–110. DOI 10.1016/j.engfracmech.2016.01.009.
22. Roychowdhury, S., Dodds, R. H. (2004). Effect of T-stress on fatigue crack closure in 3-D small-scale yielding. *International Journal of Solids & Structures, 41(9-10),* 2581–2606. DOI 10.1016/j.ijsolstr.2003.11.004.
23. Tvergaard, V. (2008). Effect of T-stress on crack growth under mixed mode I-III loading. *International Journal of Solids & Structures, 45(18),* 5181–5188. DOI 10.1016/j.ijsolstr.2008.05.014.
24. Irwin, G. R. (1948). *Fracture Dynamics, Fracturing of Metals*. Cleveland: American Society for Metals.
25. Williams, M. L. (1957). On the stress distribution at the base of a stationary crack. *Journal of Applied Mechanics, 24,* 109–114.
26. Toshio, N., Parks, D. M. (1992). Determination of elastic T-stress along three-dimensional crack fronts using an interaction integral. *International Journal of Solids & Structures, 29(13),* 1597–1611. DOI 10.1016/0020-7683(92)90011-H.
27. Hibbitt, Karlson & Sorensen Inc. (2011). *ABAQUS/Standard User's Manual Version 6.12*. Providence (RI): Hibbitt, Karlsson & Sorensen Inc.
28. CEGB. (2001). *Assessment of the Integrity of Structures Containing Defects, Revision 4*. Gloucester: British Energy Generation Ltd.
29. Milne, I., Ainsworth, R. A., Dowling, A. R., Stewart, A. T. (1988). Assessment of the integrity of structures containing defects. *International Journal of Pressure Vessels & Piping, 32(1),* 3–104. DOI 10.1016/0308-0161(88)90071-3.
30. Ainsworth, R. A. (1996). Failure assessment diagrams for use in R6 assessments for austenitic components. *International Journal of Pressure Vessels & Piping, 65(3),* 303–309. DOI 10.1016/0308-0161(94)00141-5.
31. Cicero, S., Ainsworth, R. A., Gutiérrez-Solana, F. (2010). Engineering approaches for the assessment of low constraint fracture conditions: a critical review. *Engineering Fracture Mechanics, 77(8),* 1360–1374. DOI 10.1016/j.engfracmech.2010.02.026.
32. Xing, K. T. (2015). *The Detection Report of Raw Material Span (AB span) Crane Girder of Baosteel Electric Furnace Tube Billet Casting Plant*. Beijing: China Nation Center Quality and Safety Supervision Testing of Industrial Structures (In Chinese).
33. Elgaaly, M., Nunan, W. L. (1989). Behavior of rolled section web under eccentric edge compressive loads. *Journal of Structural Engineering, 115(7),* 1561–1578. DOI 10.1061/(ASCE)0733-9445(1989)115:7(1561).
34. The Ministry of Construction of China. (2003). Code for Design of Steel Structures, GB 50017-2003. China: The Ministry of Construction of China (In Chinese).